Origin of the pressure-dependent T_c valley in superconducting simple cubic phosphorus

Xianxin Wu[*,1] Harald O. Jeschke,[1,2] Domenico Di Sante,[1] Fabian O. von Rohr,[3,4] Robert J. Cava,[3] and Ronny Thomale[1]

[1]Institut für Theoretische Physik und Astrophysik, Julius-Maximilians-Universität Würzburg, 97074 Würzburg, Germany[*]
[2]Research Institute for Interdisciplinary Science, Okayama University, Okayama 700-8530, Japan
[3]Department of Chemistry, Princeton University, Princeton, New Jersey 08544, USA
[4]Department of Chemistry, University of Zurich, CH-8057, Switzerland
(Dated: December 19, 2017)

Motivated by recent experiments, we investigate the pressure-dependent electronic structure and electron-phonon (e-ph) coupling for simple cubic phosphorus by performing first-principle calculations within the full potential linearized augmented plane wave method. As a function of increasing pressure, our calculations show a valley feature in T_c, followed by an eventual decrease for higher pressures. We demonstrate that this T_c valley at low pressures is due to two nearby Lifshitz transitions, as we analyze the band-resolved contributions to the e-ph coupling. Below the first Lifshitz transition, the phonon hardening and shrinking of the γ Fermi surface with s orbital character results in a decreased T_c with increasing pressure. After the second Lifshitz transition, the appearance of δ Fermi surfaces with 3d orbital character generate strong e-ph inter-band couplings in $\alpha\delta$ and $\beta\delta$ channels, and hence lead to an increase of T_c. For higher pressures, the phonon hardening finally dominates, and T_c decreases again. Our study reveals that the intriguing T_c valley discovered in experiment can be attributed to Lifshitz transitions, while the plateau of T_c detected at intermediate pressures appears to be beyond the scope of our analysis. This strongly suggests that besides e-ph coupling, electronic correlations along with plasmonic contributions may be relevant for simple cubic phosphorous. Our findings hint at the notion that increasing pressure can shift the low-energy orbital weight towards d character, and as such even trigger an enhanced importance of orbital-selective electronic correlations despite an increase of the overall bandwidth.

I. INTRODUCTION

Layered black phosphorus (black P), a narrow-gap semiconductor, crystallizes in the orthorhombic $A17$ structure at ambient pressure and temperature, with layers weakly bound by van der Waals forces[1,2]. The monolayer phosphorene is similar to graphene, albeit with a natural band gap[3-5]. Recently, topologically non-trivial semi-metallic properties have been discovered in the $A17$ structure at low pressure (i.e. a few GPa)[6-9], which contributed to revitalizing the interest in this material. Under pressure, early studies showed that black phosphorus exhibits several phase transitions[1,2]. The structure changes from $A17$ (orthorhombic) to semimetallic $A7$ (rhombohedral) at 4.5 GPa, followed by a metallic primitive cubic phase at 10 GPa[1,2]. The former transition is sluggish while the latter is rather sharp. It is remarkable to note that although the atoms are not closely packed[10], the primitive cubic (or simple cubic) phase is stable up to a pressure of 107 GPa before it starts to transform into a hexagonal phase, completed at 137 GPa[11]. Aside from the unusually rich variety of structural phase transitions, superconductivity was discovered in the rhombohedral and cubic phases above 5 GPa[12-14]. Put together, this naturally suggests black P to be a prime candidate for a particularly interesting shape of T_c as a function of different trajectories taken with respect to pressure and temperature. Accordingly, the pressure dependence of T_c has been investigated by many groups. Still, there is no experimental consensus on this question. This is because (i) the measured T_c appears to be strongly dependent on the path taken in P-T parameter space[13,14] and (ii), probably not uncorrelated with (i), there are mixed states due to incomplete structural phase transformations. Kawamura et al.[13,14] found that T_c increased continuously with pressure in the cubic phase on one path, while it varied only weakly with pressure around 6 K on the other path. Wittig et al.[12] discovered that T_c showed two distinct peaks at about 12 GPa and 23 GPa separated by an intriguing valley centered at about 17 GPa. In particular, Karuzawa et al.[15] showed that T_c exhibits only a single peak around 23 GPa, and the corresponding T_c was about 9.5 K. In the most recent experiment, performed with high quality black P crystals and excellent pressure cell conditions, Guo et al.[16] found a behavior similar to that of Wittig et al. in terms of pressure variation of T_c: in the cubic phase, with increasing pressure, T_c first decreases and then increases, i.e. it forms a T_c valley. From about 32 GPa, T_c exhibits a plateau for an extended pressure regime at a comparably high value. Moreover, Hall effect measurements suggested that hole carriers play an important role in promoting superconductivity, and that the T_c valley may originate from a Lifshitz transition[16].

From an initial theoretical point of view, black P does not promise to be particularly controversial. As the T_c for cubic phosphorus is relatively low (with a maximum of about 10 K) and phosphorous has an approximately half-filled p band, superconductivity has so far been assumed to be driven by electron phonon (e-ph) coupling. No consensus, however, has been reached on the pressure dependence of T_c in the cubic phase, as the result strongly depends on the adopted theoretical methods. By relating average phonon frequency and bulk modulus, early calculations[17] show a single peaked structure for T_c as a function of pressure, where the peak position is nearby the second peak of the experimental data in Ref. 12. It must be noted, however, that the variation of the phonon spectrum under pressure is completely omitted in this analysis. Other calculations have mainly focused on the elec-

tronic structure[18], or find that T_c changes little with increasing pressure[19], which is only consistent with the data on one particular path through P-T space[13]; it is inconsistent with recent experimental evidence. Another study finds that T_c increases slightly from 8.5 to 11 K as the pressure increases from 10 to 35 GPa[20], which again hardly bears similarity to experiments. A more recent, and technically significantly advanced, study involving full *ab initio* calculations of *e-ph* coupling using pseudopotentials finds that T_c decreases monotonously in the simple cubic phase[21], and reports no indication for any valley or plateau formation. Furthermore, in the latest theoretical studies, metastable structures in black P are found to be important to explain the P-T path dependent T_c in experiments[22].

In this paper, we pursue two objectives. First, facing partly contradictory experimental evidence, we attempt to consider all experimental facts on the same footing, but if in doubt center our experimental reference around Ref. 16, and apply *ab initio* methods to the most refined level in order to provide a theoretical explanation. In particular, as justified by the crystal analysis performed in Ref. 16, we explicitly start from the hypothesis that the structural transition to the simple cubic phase sets in comparably early, and that the T_c valley, as observed, occurs within this phase. By employing more reliable full-potential calculations instead of pseudopotential calculations, we attempt to resolve previous discrepancies in theoretical calculations. We manage to explain the T_c valley formation found experimentally, as the precision of our analysis allows us to disentangle effects of Lifshitz transitions from structural transitions. Second, we try to sharpen the perspective on how the *ab initio* analysis would have to be extended in order to refine the correspondence between theory and experiment. As we investigate electronic correlations in simple cubic black P, we notice several interesting aspects that might be relevant for a larger class of materials under pressure. For instance, we find that the *d*-orbital low energy weight increases as a function of pressure. In total, we are led to conclude that orbital-selective interactions as well as plasmonic contributions might provide central additional insights into the persistent intricacies of black P under pressure.

The article is organized as follows. In Section II, as also supplemented by the appendices, we introduce the detailed formalism of our *ab initio* analysis for the electronic and crystal structure as well as the *e-ph* coupling. For the former, as opposed to previous studies, we employ full potential calculations. For the latter, we likewise refine previous studies by considering band-selective *e-ph* coupling strengths. Section III proceeds by giving a detailed account on the results of our analysis for simple cubic black P. This also includes a detailed orbital-resolved study of the electronic structure, as well as the calculation of *e-ph* coupling via different *ab initio* approaches. As we are bringing together our theoretical findings with the experimental evidence in Section IV, we can quantitatively and qualitatively rationalize the T_c valley formation in the simple cubic phase. In Section V, we conclude that while we are still short of an answer to some of the experimental features, in particular to those observed for higher pressures, our systematic study supports our resulting hypothesis that electronic *ab initio* approaches are insufficient to cover the full

phenomenology of black P. Instead, we suggest that electronic correlations may enter within a degree of sophistication that is beyond such methods, and that plasmonic contributions are likely to improve the current theoretical understanding of the material.

II. METHODS

A. Electron phonon coupling formalism

We start by describing the *e-ph* coupling formalism we employ. The *e-ph* matrix element for the scattering of an electron in band n at wave vector $\mathbf{k}$ to a state in band m with wave vector $\mathbf{k} + \mathbf{q}$, with the absorption or emission of a phonon with mode ν at wave vector $\mathbf{q}$, is

$$g_{mn}^{\nu}(\mathbf{k}, \mathbf{q}) = \sqrt{\frac{\hbar}{2M\omega_{\mathbf{q}\nu}}} \langle m, \mathbf{k} + \mathbf{q}|\delta_{\mathbf{q}\nu} V_{SCF}|n, \mathbf{k}\rangle . \quad (1)$$

In (1), $|n, \mathbf{k}\rangle$ is the electronic Bloch state, $\omega_{\mathbf{q}\nu}$ is the screened phonon frequency, M is the atomic mass, and $\delta_{\mathbf{q}\nu} V_{SCF}$ is the derivative of the self-consistent potential with respect to the collective atomic displacements corresponding to phonon mode ν at wave vector $\mathbf{q}$. The phonon self energy is given by

$$\Pi_{\mathbf{q}\nu} = \frac{1}{N_{\boldsymbol{k}}} \sum_{mn,\mathbf{k}} |g_{mn}^{\nu}(\mathbf{k}, \mathbf{q})|^2 \frac{n_{\mathrm{F}}(\epsilon_{m\mathbf{k}+\mathbf{q}}) - n_{\mathrm{F}}(\epsilon_{n\mathbf{k}})}{\omega_{\mathbf{q}\nu} + i\delta + \epsilon_{m\mathbf{k}+\mathbf{q}} - \epsilon_{n\mathbf{k}}} , \quad (2)$$

where $\epsilon_{n\mathbf{k}}$ is the energy relative to the Fermi level for the Bloch state, $n_{\mathrm{F}}(\epsilon)$ is the Fermi distribution function and $N_{\boldsymbol{k}}$ is the number of k points. The phonon linewidth is proportional to the imaginary part of the phonon self energy. Considering the large value of the Fermi energy compared to the phonon frequencies, the phonon linewidth at low temperature can be written as[23]

$$\gamma_{\mathbf{q}\nu}(\omega) = \frac{2\pi\omega_{\mathbf{q}\nu}}{N_{\boldsymbol{k}}} \sum_{mn,\mathbf{k}} |g_{mn}^{\nu}(\mathbf{k}, \mathbf{q})|^2 \delta(\epsilon_{m\mathbf{k}+\mathbf{q}})\delta(\epsilon_{n\mathbf{k}}) . \quad (3)$$

The *e-ph* coupling constant for a specific phonon mode is,

$$\lambda_{\mathbf{q}\nu} = \frac{\gamma_{\mathbf{q}\nu}}{\pi N(E_{\mathrm{F}})\omega_{\mathbf{q}\nu}^2} , \quad (4)$$

where $N(E_{\mathrm{F}})$ is the density of states per spin at the Fermi level. In terms of the phonon linewidths, the Eliashberg spectral function $\alpha^2 F(\omega)$ can be written as

$$\alpha^2 F(\omega) = \frac{1}{2\pi N(E_{\mathrm{F}})} \sum_{\mathbf{q}\nu} \frac{\gamma_{\mathbf{q}\nu}}{\omega_{\mathbf{q}\nu}} \delta(\omega - \omega_{\mathbf{q}\nu}) . \quad (5)$$

Finally, the isotropic *e-ph* coupling constant is defined as

$$\lambda = 2 \int_0^{\infty} d\omega \frac{\alpha^2 F(\omega)}{\omega} . \quad (6)$$

For multiband systems, as is the case for simple cubic P, it is useful to introduce a band-resolved *e-ph* coupling constant

c_{mn}, which describes the Cooper pair scattering of an electron from band m to band n by phonons, and is defined as[24]

$$c_{mn} = V_{mn}N_m N_n$$
$$= \frac{2}{N_q N_k} \sum_{\substack{k \in n, k+q \in m, \nu}} \omega_{q\nu}^{-1}|g_{mn}^{\nu}(\mathbf{k}, \mathbf{q})|^2 \delta(\epsilon_{m\mathbf{k+q}})\delta(\epsilon_{n\mathbf{k}}),$$

(7)

where N_m (N_n) is the DOS at the Fermi level contributed by m-th (n-th) band and V_{mn} is the effective interaction for Cooper pair scattering. The isotropic e-ph coupling constant can be written as

$$\lambda = \sum_{mn} \frac{c_{mn}}{N(E_F)} = \sum_{mn} \frac{V_{mn}N_m N_n}{N(E_F)}. \quad (8)$$

In multiband systems, the e-ph constant is given by the maximum eigenvalue λ_{multi} of the matrix Λ, which is defined as

$$\Lambda_{mn} = V_{mn}N_n = \frac{c_{mn}}{N_m}. \quad (9)$$

The band-resolved Eliashberg function $\alpha^2 F_{mn}(\omega)$ reads

$$\alpha^2 F_{mn}(\omega)$$
$$= \sum_{\substack{k \in n, k+q \in m, \nu}} \frac{|g_{mn}^{\nu}(\mathbf{k}, \mathbf{q})|^2 \delta(\epsilon_{m\mathbf{k+q}})\delta(\epsilon_{n\mathbf{k}})\delta(\omega - \omega_{q\nu})}{N_n N_q N_k}.$$

(10)

Then, the matrix element Λ_{mn} can be written as

$$\Lambda_{mn} = 2 \int_0^\infty d\omega \frac{\alpha^2 F_{mn}(\omega)}{\omega}. \quad (11)$$

T_c can be determined using the Allen-Dynes-modified McMillan equation[25,26],

$$T_c = \frac{\omega_{ln}}{1.2} \exp\left\{ -\frac{1.04(1+\lambda)}{\lambda - \mu^*(1+0.62\lambda)} \right\}, \quad (12)$$

where μ^* is the Coulomb pseudopotential[27] and λ is the isotropic (or multi-band) e-ph coupling constant. ω_{ln} is defined as

$$\omega_{ln} = \exp\left\{ \frac{2}{\lambda} \int_0^\infty d\omega \ln\omega \frac{\alpha^2 F(\omega)}{\omega} \right\}. \quad (13)$$

Using Eq. 12, we obtain T_c based on a suitable choice of μ^* and compare with previous works. However, we also use the solution of the isotropic Eliashberg equations to determine T_c without any empirical parameters[28,29].

B. Details of the calculations

In the relaxation with external pressure, we employ the projector augmented wave (PAW) method[30] as implemented in the Vienna ab initio simulation package (VASP)[31–33], where both the local density approximation (LDA) and

the generalized-gradient approximation (GGA)[34] for the exchange correlation functional are used. The expansion of the wave functions in the plane-wave basis is cut off at 600 eV. The adopted k-point mesh is $37 \times 37 \times 37$ and the convergence criterion is that all the forces on atoms are less than 0.001 eV/Å. The e-ph coupling calculations are performed with the full-potential linear augmented plane wave (FP-LAPW) method[35] as implemented in the Elk code[36,37]. In the calculations, we chose the Perdew-Burke-Ernzerhof (PBE) exchange correlation functional. The adopted muffin-tin radii R_{MT} (2.05-2.20 a.u.) for P depend on the lattice constants and the plane-wave cutoff is set to $R_{\text{MT}} \times k_{\text{max}} = 8.5$. The angular momentum expansion in the muffin tins is taken to $l_{\text{max}} = 12$ for both the wave functions and the potential. We use the full potential local orbital (FPLO) basis[38] as a further accuracy check for the electronic structure. For accurate DOS calculations, we use $\mathbf{k}$-point meshes of $100 \times 100 \times 100$. Phonon dispersions are obtained by using the supercell method, and we have carefully checked the convergence of the phonon spectrum with respect to q-point mesh. We find that an $8 \times 8 \times 8$ q-point mesh is enough to obtain the converged phonon spectrum. For the phonon linewidth in Eq. 3, in Elk the δ function is numerically replaced by a Gaussian function with a smearing parameter σ. The convergence of $\gamma_{\nu q}$ with respect to k-point mesh has also been carefully checked, and the final results are obtained from calculations with a $128 \times 128 \times 128$ k-point mesh and $\sigma = 0.004\,\text{Ha} \approx 100\,\text{meV}$. With the chosen parameters, λ is estimated to converge within 0.01 (i.e. less than 2%). We also perform e-ph calculations to obtain the resistivity by using the EPW (short for electron-phonon coupling using Wannier functions) method[39,40], as implemented in the Quantum Espresso pseudopotential plane wave code package[41].

III. RESULTS

A. Crystal and electronic structure for simple cubic phosphorous

The calculated lattice constants as a function of external pressure for simple cubic phosphorus are shown in Fig. 1, in comparison with experimental data[16,42]. The lattice constants from PBE are always slightly larger than those of LDA. From the figure, we find that the calculated lattice constants from PBE matches better with available experimental data, suggesting that the PBE functional may be more suitable for P than the LDA functional. Therefore, we adopted the PBE functional in all further calculations. The total density of states (DOS) and the orbital projected DOS are shown in Fig. 2. At ambient pressure, the states near the Fermi level E_F are mainly formed by p-orbitals. As the pressure increases, however, the total states display shifts to lower energy, and the contribution from p-orbital and s-orbital states at E_F decreases while the d-orbital weight increases. The DOS at the Fermi level $N(E_F)$ as a function of external pressure is shown in Fig. 3 (a). We find that $N(E_F)$ first decreases linearly, and then increases with the increase of external pres-
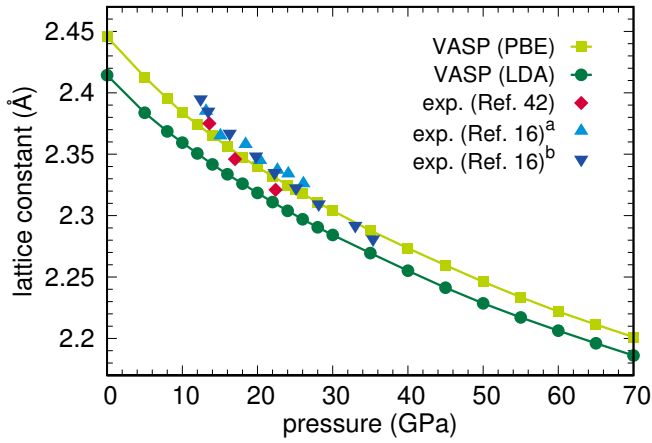
FIG. 1: (Color online) Theoretical and experimental lattice constants as a function of external pressure for simple cubic phosphorous. Calculations are performed with VASP using two different exchange correlation functionals, and experimental data are taken from Ref. 42 and Ref. 16 ([a] and [b] refer to two different runs).
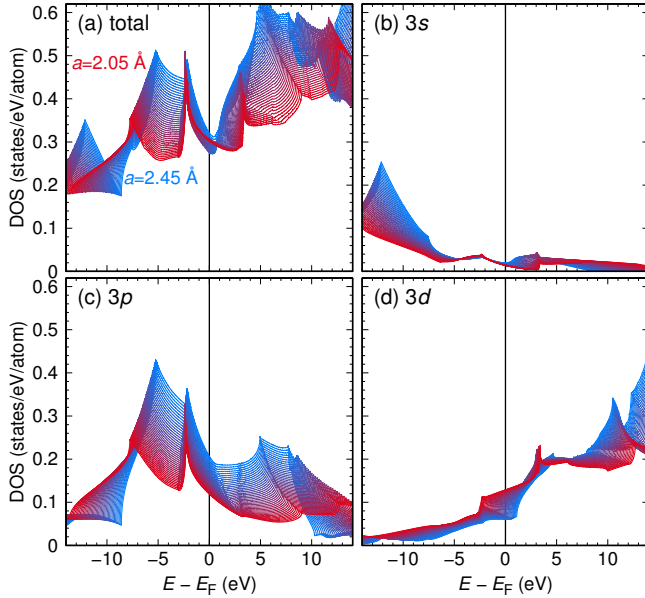

FIG. 2: (Color online) Total and orbital projected densities of states in the simple cubic phase for various lattice constants. This calculation was done with FPLO. The gradient lines ranging from blue to red represent the increasing of pressures (decreasing of lattice constantsp).
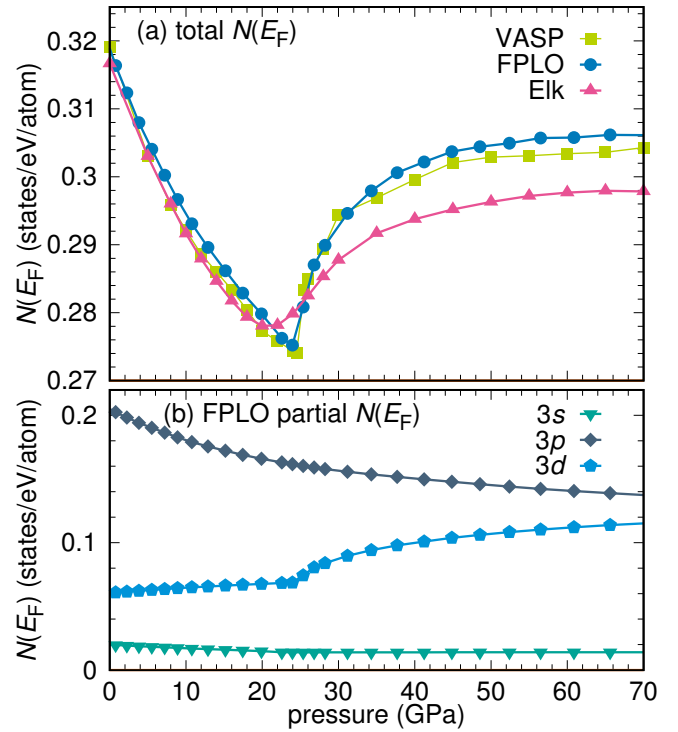

FIG. 3: (Color online) Density of states at the Fermi level for the simple cubic phase as a function of external pressure. (a) Comparison between different basis sets. (b) Orbital contributions to $N(E_F)$.

sure, which results in a local minimum in $N(E_F)$. The corresponding pressure is 22 GPa ($a = 2.332$ Å) in PBE calculations. The $N(E_F)$ we obtain as function of pressure in principle compares well with previous calculations[17,21] but has a more pronounced minimum. The orbitally resolved $N(E_F)$ in Fig. 3 (b) shows that the $3d$ orbital is responsible for the increase of $N(E_F)$ beyond the minimum at $P = 22$ GPa; taking only s and p orbitals into account, $N(E_F)$ would fall monotonously.

To explain the observed changes in the DOS, we plot the orbital projected band structures for external pressures of $P = 10$ GPa, 22 GPa, 40 GPa and 70 GPa in Fig. 4. We find that the major changes at the Fermi level occur in bands with s and d, rather than p character. At the R point, a band with s character which is partially occupied below 22 GPa shifts up in energy with increasing pressure, while a band around M with d character changes with pressure in an opposite fashion, and starts to become populated around $P = 22$ GPa. These changes are consistent with previous calculations[17,18,21]. The corresponding Fermi surfaces (FSs) at these pressures are shown in Fig. 5. At 10 GPa, close to the rhombohedral-simple cubic phase transition point in experiment, there are three FSs: a cubic hole FS α around Γ, a big open-type FS β and a small spherical electron FS γ. The α and β FSs are attributed to p orbitals and enclose about 0.07 holes and 1.068 electrons (or 0.932 holes), respectively. The band contributing to the β FS is close to half filling. The γ FS, predominantly formed by s orbitals, encloses about 0.002 electrons. As pressure increases, the γ FS gradually shrinks and the β FS grows a bit while the α FS remains almost unchanged. At $P = 22$ GPa, the γ FSs disappear completely, and the Lifshitz transition occurs. With a slight further increase of pressure, three ellipsoidal electron FSs δ appear around M. Two Lifshitz transitions happen almost at the same pressure and, as it turns out, have a significant effect on the e-ph coupling. The δ FSs are of d orbital character, as expected from the bandstructures in Fig. 4. As correlation effects in d orbitals are stronger as
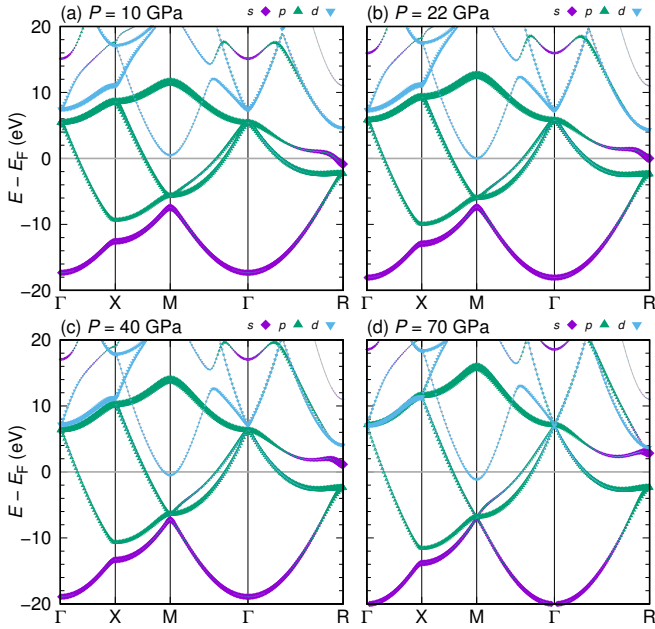
FIG. 4: (Color online) Band structures with orbital weights for simple cubic phosphorous at four different external pressures.
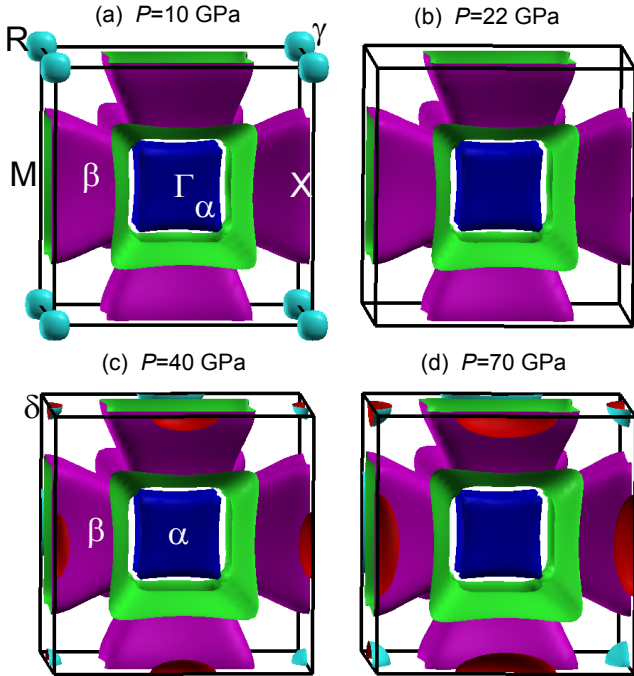

FIG. 5: (Color online) The Fermi surfaces for external pressures P=10 (a), 22 (b), 40 (c) and 70 GPa (d).
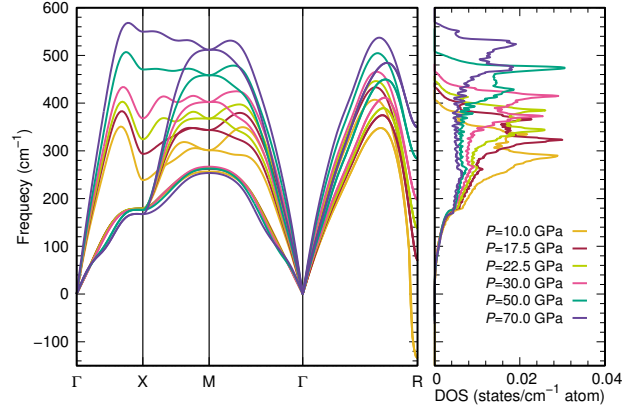

FIG. 6: (Color online) Phonon spectra and densities of states for simple cubic phosphorus at several pressures.

band structures are given in Appendix A. In calculations with the hybrid functional, the bandwidth increases and the most noticeable changes near the Fermi level are that the s band at R and the d band at M are are shifted to slightly higher energy, and as a consequence the two Lifshitz transitions happen separately. In GGA+U calculations, however, the obtained band structures are almost unchanged compared to the GGA functional. Therefore, correlations have little effect on the band structure, but may still have a significant effect on the superconductivity of phosphorus.

B. Electron phonon coupling for cubic phosphorous

Now we turn to the effect of pressure on the phonons for simple cubic phosphorus. The phonon spectra and densities of states are shown in Fig. 6 for several pressures. Below $P = 16$ GPa, there are imaginary phonon modes around the R point. The unstable modes correspond to the lattice distortion in the direction of the rhombohedral $A7$ phase[21]. Above $P = 16$ GPa, unstable phonon modes vanish and most phonon states lie in two regions: A low-energy region (LER) and a high-energy region (HER). DOS is small in the LER but shows large peaks in the HER; the latter contains more states than the former. At 17.5 GPa, for example, the LER is from 180 cm^{-1} to 280 cm^{-1} and the HER is from 280 cm^{-1} to 400 cm^{-1}. In the LER, phonon bands are relatively smooth, and phonon states are mainly due to phonon modes around Γ and R as well as low-energy modes around X and M. In the HER, the situation is quite different. Along the $\Gamma - X$ direction, the frequency of the longitudinal mode increases and reaches a maximum near the X point, to then drop suddenly. One mode along $\Gamma - M$ and three modes along $\Gamma - R$ direction exhibit similar behavior, and the drops near the R point are the largest. All this finally results in a large DOS in the HER. As pressure increases, the drops near X, M, and R decrease and most phonon modes harden, which leads to the widening of the LER and a shift towards higher frequency for the HER. These changes have a significant effect on the e-ph coupling discussed in the following.

compared to p orbitals, the appearance of the δ FSs around M may trigger stronger electronic correlation effects. This runs contrary to the expectation that pressure increases the bandwidth, and thus should decrease correlation effects as a matter of principle. To investigate the correlation effects, we performed calculations with hybrid functional and GGA+U. The

To investigate the *e-ph* coupling for simple cubic phosphorus, we first plot the phonon linewidth at two instructive values of pressure (before and after the Lifshitz transitions) in Fig. 7. Strong *e-ph* coupling occurs in the high-energy modes around X and M and all modes around R, which is due to the large Fermi-surface nesting at these $\boldsymbol{q}$ vectors[21]. With the increase of pressure, the phonon linewidth near X, M and R increases a little bit. The obtained $\lambda_{\nu\boldsymbol{q}}$ along high symmetry k-points for four pressures are shown in Fig. 8. The *e-ph* coupling constant $\lambda_{\nu\boldsymbol{q}}$ is peaked at R. It is rather different from the distribution of phonon linewidths $\gamma_{\nu\boldsymbol{q}}$, where γ_{3M} and γ_{3X} are comparable with γ_R. As the phonon frequencies at R are lower than those at X and M, and since $\lambda_{\nu\boldsymbol{q}}$ is inversely proportional to $\omega_{\nu\boldsymbol{q}}^2$, the λ_X and λ_M are much smaller than λ_R. Most $\lambda_{\nu\boldsymbol{q}}$ decrease with increasing pressure. However, contrary to the pressure-dependent behavior of $\lambda_{\nu\boldsymbol{q}}$ around X, M and R, after the Lifshitz transitions the $\lambda_{1\boldsymbol{q}}$ and $\lambda_{2\boldsymbol{q}}$ around Γ (along $\Gamma - X$, $\Gamma - M$ and $\Gamma - R$ directions) increase with increasing pressure, which can be attributed to the softening of phonon modes at these $\boldsymbol{q}$ vectors. These features are consistent with the previous plane wave pseudopotential calculation[21].

In order to analyze the contributions of different Fermi surfaces to the *e-ph* coupling, we plot the band resolved Eliashberg spectral functions in Fig. 9. Before the Lifshitz transition, at $P = 17.5$ GPa the $\beta\beta$ intraband coupling and $\alpha\beta$ interband coupling contribute dominantly to *e-ph* coupling, which is due to the large β Fermi surfaces and relative good nesting between α and β Fermi surfaces. As the spherical γ FS is well separated from α and β FS in k-space, the $\alpha\gamma$ and $\beta\gamma$ interband couplings are relatively weak. Upon increasing pressure, the peak of $\beta\beta$ intraband coupling becomes broad and shifts to higher frequency, which results in a significant *e-ph* coupling decrease in the $\beta\beta$ channel. At the Lifshitz transition point, the $\alpha\gamma$ and $\beta\gamma$ interband couplings vanish due to the disappearance of the γ FS. Thus, *e-ph* coupling decreases with increasing pressure before the Lifshitz transition, as shown in Fig. 11. As pressure further increases, three δ FSs with d orbital character appear around the M point, and they introduce strong interband couplings in $\alpha\delta$ and $\beta\delta$ channels (see Fig. 9 (c)), similar to the case of sulfur under pressure[43]. The *e-ph* coupling increases with increasing pressure because the *e-ph* coupling enhancements from new channels overcome the weakening of couplings in $\alpha\beta$ and $\beta\beta$ channels. Therefore, λ exhibits a valley around the Lifshitz transition point. After the Lifshitz point, the isotropic λ increases and reaches a maximum at $P = 30$ GPa. As pressure further increases, the two broad peaks in $\beta\delta$ channels show opposite behaviors: one shifts to higher frequency and the other shifts to lower frequency. The remaining interband and intraband *e-ph* couplings shift to higher frequency. This will lead to decreased *e-ph* couplings in most channels except the $\delta\delta$ intraband channel. Therefore, λ will decrease again.

The isotropic Eliashberg spectral functions $\alpha^2 F(\omega)$ at five selected pressures are shown in Fig. 10. We find that the $\alpha^2 F(\omega)$ have almost the same shapes as the phonon DOS shown in Fig. 6. The *e-ph* coupling occurs mainly in the high energy region and it is mainly due to $\beta\beta$ intraband coupling

and $\alpha\beta$, $\alpha\delta$ and $\beta\delta$ interband coupling. This high energy spectral weight shifts to higher frequency with increasing pressure, rather similar to the behavior of the phonon DOS. Another noticeable feature in $\alpha^2 F(\omega)$ is that the *e-ph* coupling ($100 cm^{-1}$ to $200 cm^{-1}$) in the low energy region increases as pressure increases, which can be mainly attributed to *e-ph* coupling in the $\beta\delta$ channel.

We calculate T_c using the McMillan equation (Eq. 12) and the Coulomb pseudopotential parameter μ^* is fixed to $\mu^*=0.12$, a a value for μ^* that matches the minimum T_c in our calculations to the experimentally determined T_c valley observed in Ref. 16. This μ^* is significantly smaller than that in Ref. 21. We also calculate T_c by solving the isotropic Eliashberg equations self-consistently[28]. Fig. 11 shows the calculated isotropic *e-ph* coupling constant λ, multi-band *e-ph* coupling constant λ_{multi}, and T_c as a function of pressure in theory, compared to the experimental data from different groups. The multi-band *e-ph* coupling constant and T_c are larger than the corresponding isotropic ones. With increasing pressure, the isotropic and multi-band λ and T_c first decrease and then increase, thus form a valley, and finally decrease again. We also performed calculations using EPW, where the trend of pressure dependent λ and T_c turns out to be rather similar (see Appendix B). The obtained λ are close to those in Ref. 17–19 but smaller than those in Ref. 21. The origin of this difference is unclear, and may be related to an inherent difference of the approaches. Overall, the trend as a function of pressure is not consistent with the recent *e-ph* coupling calculations using a Wannier interpolation approach[21], where a large smearing parameter σ (0.27 eV) is adopted which significantly overestimates T_c before the Lifshitz transitions.

From our theory, the calculated T_c exhibits a valley formation similar to Ref. 16 depicted as down-triangles in Fig. 11, as it is also consistent with the data in Ref. 12 (green squares) in the range from $P = 5$ GPa to $P = 25$ GPa. While our calculations can thus explain the observed T_c valley, the most prominent feature in recent experiments, they do not explain the plateau seen in Ref. 16 beyond $P = 32$ GPa. The T_c valley can be attributed to the Lifshitz transitions, which is also consistent with the Hall measurements[16]. The pressure for the T_c minimum in experiment and our theoretical calculations are at 17 GPa and 22 GPa, respectively. The difference is relatively small, and can be decreased if we include correlation effects in the calculations. Two state of the art methods, pseudopotential calculations combined with Wannier function interpolation and full potential all-electron calculations, arrive at the same result which can successfully explain the T_c valley formation.

IV. DISCUSSION

Above 5 GPa, when orthorhombic black phosphorus partially converts to the rhombohedral phase, superconductivity appears. In the mixed phase region, T_c increases. At 12 GPa, the rhombohedral phase transforms into the cubic phase, and T_c shows a jump[16]. Our calculations indicate that the phase transition happens at 19 GPa (see Appendix C), which
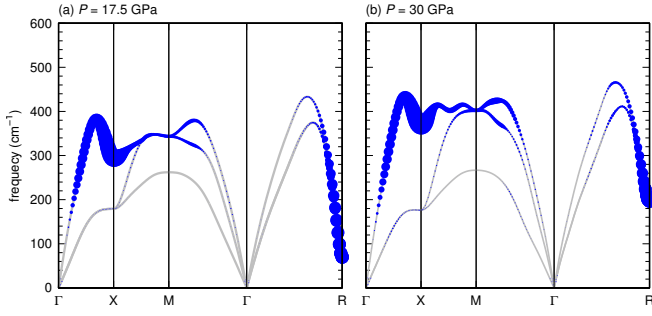
FIG. 7: (Color online) The phonon linewidth $\gamma_{\nu q}$ along high symmetry q-points at P=17.5 GPa (before the Lifshitz transition) and P=30 GPa (after the Lifshitz transition). The sizes of the circles represent the magnitude of $\gamma_{\nu q}$.
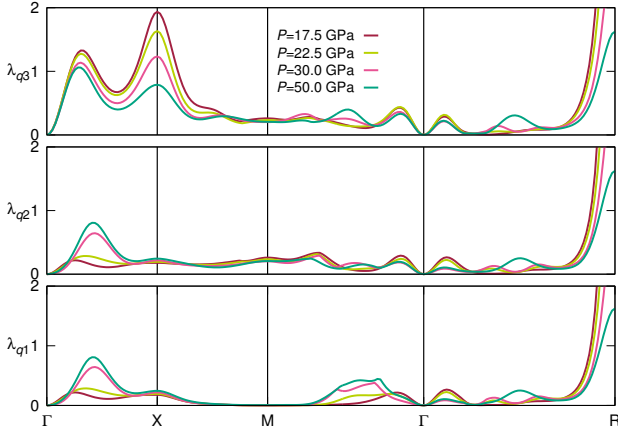

FIG. 8: (Color online) Electron phonon coupling constant $\lambda_{\nu q}$ along high symmetry q directions at $P = 17.5$ GPa, 22.5 GPa, 30.0 GPa and 50.0 GPa.
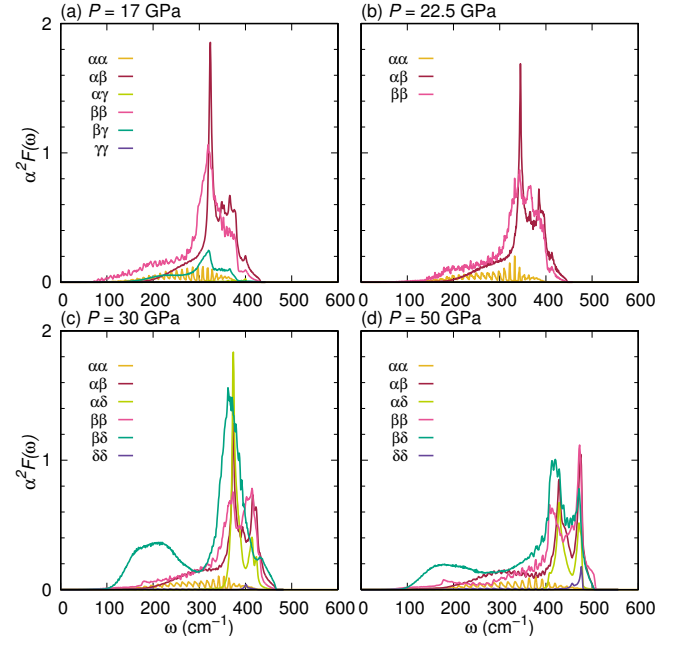

FIG. 9: (Color online) Band-resolved Eliashberg spectral function $\alpha^2 F_{mn}(\omega)$ for cubic phosphorus at $P = 17.5$ GPa, 22.5 GPa, 30.0 GPa and 50.0 GPa.
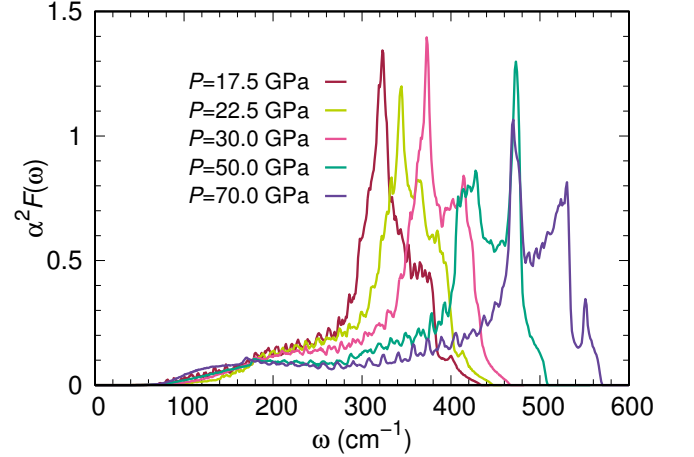

FIG. 10: (Color online) Eliashberg spectral function $\alpha^2 F(\omega)$ for cubic phosphorus at $P = 17.5$ GPa (a=2.350 Å), 22.5 GPa (a=2.330 Å), 30.0 GPa (a=2.300 Å), 50.0 GPa (a=2.246 Å) and 70.0 GPa (a=2.201 Å).

is higher than that in experiment. Moreover, the couplings between p orbitals along [111] direction in the cubic phase are uniform compared with those in the rhombohedral phase due to its high-symmetry structure, which suppresses band splitting near the Fermi level, and hence results in a higher $N(E_f)$. Therefore, $N(E_f)$ shows a jump across the structural phase transitions, which directly feeds into the value of T_c. Furthermore, we perform phonon calculations in both phases at 22 GPa, where d orbital bands are still not involved. The phonon spectra are given in Appendix C. Due to the change in crystal symmetry at the phase transition, in the cubic phase there are more degenerate phonon modes and the phonons soften a little compared with the rhombohedral phase. This leads to an increased e-ph coupling constant and T_c shows a jump of about 1.3 K with $\mu^* = 0.12$. It is consistent with experimental data in Ref. 16, which shows that the structural phase transition taking place at 12.4 GPa is accompanied by a jump in T_c. At this low pressure, the Lifshitz transition cannot occur according to our calculations. Therefore, the T_c jump across the phase transition should be mainly attributed to the change in crystal symmetry rather than the Lifshitz transition.

In the normal state, simple cubic phosphorus exhibits a quadratic temperature dependence of the resistance in the normal state, and resistance decreases as pressure increases[16]. The resistance due to e-ph coupling can be expressed as[44],

$$\rho(T) = \frac{4\pi m_e}{ne^2 k_B T} \int_0^\infty d\omega \hbar \omega \alpha_{\mathrm{tr}}^2 F(\omega) n(\omega, T)[1 + n(\omega, T)], \tag{14}$$

where $n(\omega, T)$ is the Bose-Einstein distribution. The Eliashberg transport coupling function is similarly defined as the Eliashberg spectral function[44]. According to our calculations, the shape of $\alpha_{\mathrm{tr}}^2 F(\omega)$ is very similar to that of $\alpha^2 F(\omega)$, and with increasing pressure $\alpha_{\mathrm{tr}}^2 F(\omega)$ exhibits similar behavior
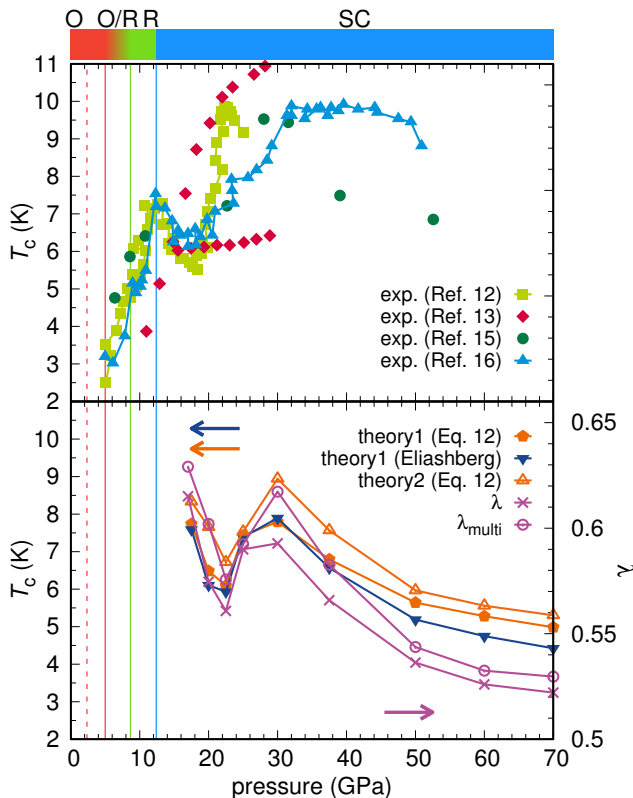
8

FIG. 11: (Color online) Superconducting transition temperature T_c and e-ph coupling constant λ as a function of pressure in theoretical calculations compared to the experimental data. Squares, circles, diamonds and triangles denote the data from J. Wittig *et al.*[12], Karuzawa *et al.*[15], Kawamura *et al.*[13] and Guo *et al.*[16], respectively. "theory1" denotes T_c from the isotropic λ and "theory2" denotes T_c from the multi-band λ_{multi}.

FIG. 12: (Color online) Temperature dependent resistivity for cubic phosphorus from e-ph coupling.

in part attributed to that. Instead, starting from the hypothesis that we take this precise shape of T_c as reference, one possible explanation could be that electronic correlations may contribute to superconductivity in simple cubic phosphorus at high pressure. From the analysis above, we know that electron pockets around the M points are mostly composed of d orbitals, and appear when $P > 22$ GPa. The electronic correlation effects in d orbitals are expected to be stronger than those in p and s orbitals. As such, these correlation effects should become more and more important at high pressures, even though the overall bandwidth increases. Assuming that electron-electron interactions might participate in the pairing mechanism on these Fermi surfaces, with increasing pressure, the δ Fermi surfaces grow bigger, and the carrier density of electrons with d orbital character increases (see Fig. 2), which could enhance the Cooper pairing. This will further enlarge the pressure region where T_c increases. If the enhancement from correlation effects can make up for the T_c decrease due to phonon hardening, it may lead to such a T_c plateau at high pressure. In Ref. 22, where electronic interactions have been considered within the static random phase approximation (RPA), one could not reproduce the experimentally observed behavior of T_c at high pressure. This suggests that effects which are beyond the static RPA level need to be taken into account. One possibility is that the frequency dependence of the interaction is important, and that plasmons, which can cooperate with phonons and significantly raise T_c, provide an explanation[45].

V. CONCLUSIONS

We have investigated the electronic structure and electron phonon coupling for simple cubic phosphorus by performing first-principle calculations within the FP-LAPW method. Our calculations show that with increasing pressure, T_c first decreases, then increases and so forms a valley, and then decreases again. Before the Lifshitz transitions set in, the

compared to $\alpha^2 F(\omega)$. It will lead to a decreased resistance with increasing pressure, as shown in Fig. 12, which is consistent with the experimental data both in its temperature and its pressure dependence. This suggests that e-ph coupling has a significant contribution to the electrical resistance.

Our calculations can successfully explain the observed T_c valley in the simple cubic phase but not the T_c plateau at high pressure. The T_c valley in experiment turns out to have an electronic origin, as it is due to Lifshitz transitions. At high pressure, the phonon modes harden rapidly, and the e-ph coupling constant as well as T_c decrease with increasing pressure in our calculations, which is inconsistent with the observed T_c plateau as a rather high value. If we study how T_c evolves in experiment for higher pressure, one finds that T_c remains almost unchanged for an extended regime of varying pressure, while the hole carrier density decreases for $P > 30$ GPa. Such evidence is rather intriguing, and hard to explain. Let us first note that systematic errors in the actual pressure imposed on the crystal might in fact be bigger for higher than for lower pressures. As a consequence, it potentially cannot be excluded that the increased pressure is not homogeneously imposed on the whole crystal, and that the plateau might be
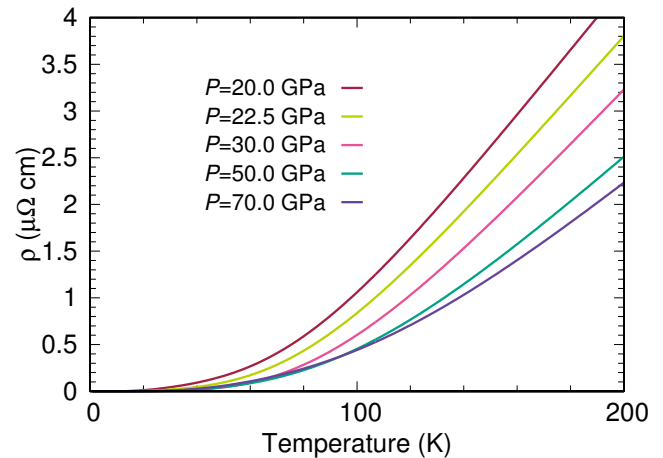
phonon hardening and shrinking of the γ Fermi surface result in a decrease of T_c with increasing pressure. After the Lifshitz transitions, the appearance of δ Fermi surfaces with $3d$ orbital character generates strong electron-phonon interband couplings in $\alpha\delta$ and $\beta\delta$ channels, and hence increases T_c. With further increase of pressure, phonon hardening makes a dominant contribution to electron-phonon coupling, and T_c decreases again. Our study reveals that the intriguing T_c valley, as found in experiment should be attributed to the Lifshitz transitions. We also find, however, that the experimentally observed T_c plateau at high pressure is beyond the electron-phonon mechanism considered here. It suggests that besides electron-phonon coupling, plasmonic contributions along with electronic correlations may be relevant for systems with d-orbital character at higher pressures, such as for simple cubic black phosphorous.

FIG. 13: (Color online) Band structures with GGA functional and hybrid functional (HSE06) for simple cubic phosphorous at four different external pressures.

Acknowledgments

Appendix A: Band structures for simple cubic phosphorus with GGA+U and HSE

According to our calculations, a band with d orbital character will cross the Fermi level at sufficiently high pressure. This suggests that correlation effects may be important in simple cubic phosphorus, and we check if they have an important effect on the electronic structure. First, we perform calculations with a hybrid functional (HSE06)[46]; the obtained band structures are shown in Fig. 13 in comparison with GGA bands. Compared to the bands calculated with GGA functional, the bandwidth in HSE band increases, and the most noticeable changes near the Fermi level are that the s band at R and the d band at M are are shifted to slightly higher energies. The two Lifshitz transitions at the R and M points occur at almost the same pressure in GGA calculations but happen at 20 GPa and 38 GPa in HSE calculations.

We also tried to consider the local interaction by performing a GGA+U calculation. The adopted U and J are 2.0 eV and 0.5 eV for p orbital and d orbital, respectively. The band structures are given in Fig. 15. No matter whether the additional U
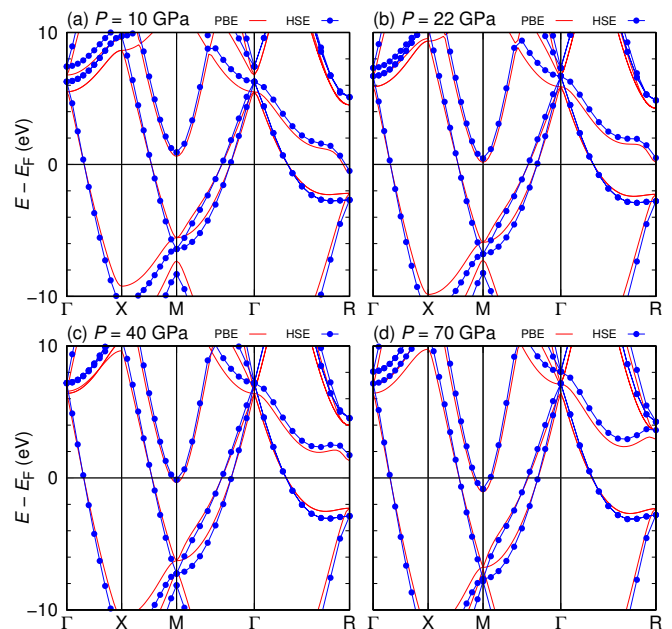
interaction is on p or d orbitals, the obtained band structures are almost the same as those with GGA functional. Therefore, GGA+U has little effect on the band structures of simple cubic phosphorus. Furthermore, we calculate the phonon spectra for phosphorus at 20 GPa and 25 GPa, and the phonon dispersions are shown in Fig. 15. The phonon modes in GGA+U calculations soften a little bit compared with those in GGA calculations. This phonon softening will increase the e-ph coupling but cannot change the general negative trend of the pressure-dependent e-ph coupling constant.

Appendix B: Electron-phonon coupling constant and T_c from EPW

We also perform electron-phonon coupling calculations using EPW. To obtain the nine Wannier functions, we use the Bloch functions on an $8 \times 8 \times 8$ k mesh. Phonon dispersions are calculated on an $8 \times 8 \times 8$ q-mesh using density functional perturbation theory. For the e-ph calculations, a very fine $128 \times 128 \times 128$ k mesh and a $24 \times 24 \times 24$ q mesh are used, and the δ function in the phonon linewidth is approximated by Gaussian functions with $\sigma = 0.08$ eV. After obtaining good Wannier functions, which can be used to reproduce the first-principle band structures and phonon dispersions with high accuracy, we perform electron-phonon calculations. The obtained electron-phonon coupling constant and T_c are shown in Fig. 18. Similar to the results from elk, both λ and T_c first decrease then increase, forming a valley, and decrease again with increasing pressure. Therefore, both elk and EPW calculations confirm that there is a T_c valley in the superconducting T_c versus pressure phase diagram, which can be attributed to
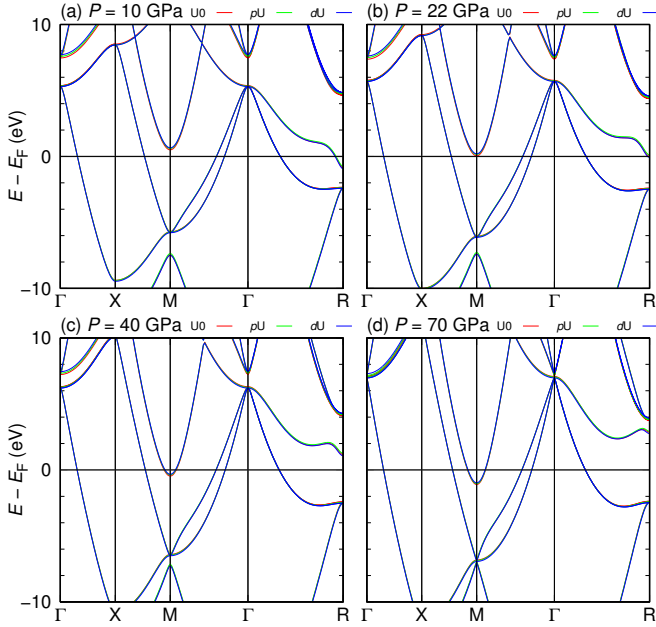
FIG. 14: (Color online) The band structures with GGA+U for simple cubic phosphorous at four different external pressures. $U0$ represent GGA calculations, pU and dU represent that in GGA+U calculations the additional U is on p orbital and d orbital, respectively.
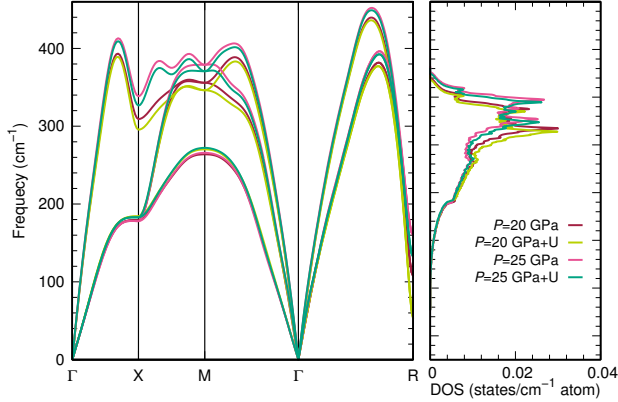

FIG. 15: (Color online) Phonon spectra and densities of states with GGA and GGA+U for simple cubic phosphorus at $P = 20$ GPa and $P = 25$ GPa.

the Lifshitz transitions. The results are consistent with those from elk calculations.

Appendix C: Density of states evolution from rhombohedral to cubic phosphorus

While we have focused on simple cubic phosphorous in this work as it is the phase with the highest superconducting transition temperature, it is also interesting how the transition to the high T_c phase occurs. We first investigate the stability of rhombohedral phosphorus relative to simple cubic phospho-
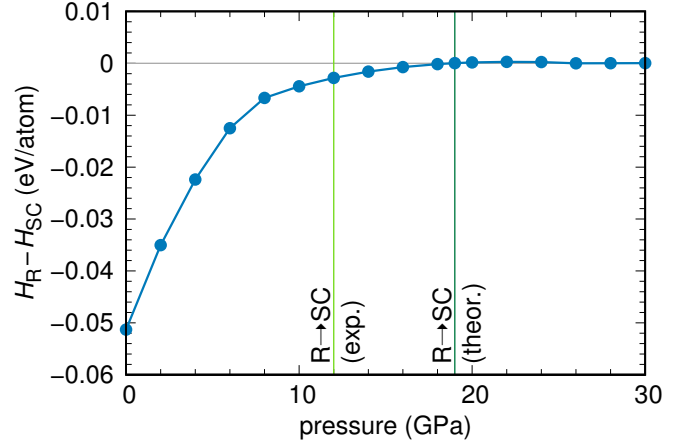

FIG. 16: (Color online) Enthalpy for rhombohedral phosphorus relative to the simple cubic phase as a function of pressure.
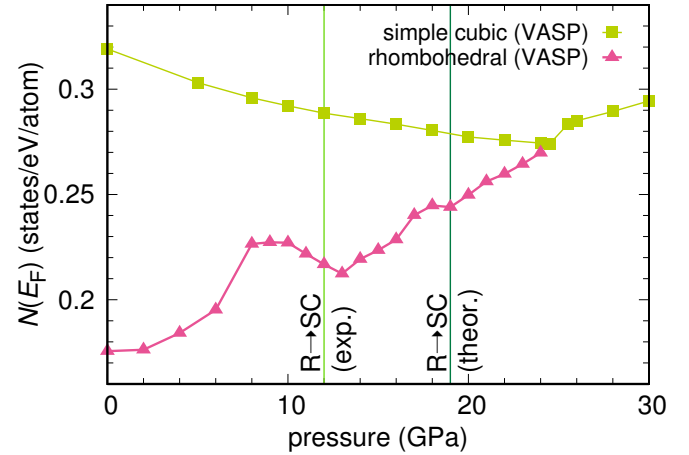

FIG. 17: (Color online) Density of states at the Fermi level for the simple cubic and rhombohedral phases as a function of pressure.

rus by calculating enthalpies as a function of external pressure; the difference between enthalpies in simple cubic and rhombohedral phases is shown in Fig. 16. Below 9 Gpa, the dominant structure is orthorhombic but here we focus on the cubic and rhombohedral phases above 10 GPa. From our calculations, the enthalpies of the two phase are very close above 10 GPa and the rhombohedral to simple cubic phase transition occurs at 19 GPa, which is consistent with previous calculations[21]. This transition pressure is higher than the 12 GPa observed in experiment[16]. Fig. 17 shows the DOS at the Fermi level for simple cubic and rhombohedral phases as a function of pressure. At the phase transition, the density of states at the Fermi level $N(E_F)$ jumps up sharply (both at the experimental and at the theoretical transition pressures). As T_c is often proportional to $e^{-\frac{1}{VN(E_F)}}$, the jump of $N(E_F)$ can lead to a jump in T_c, which explains the observed T_c jump across the phase transition in experiments[16]. Moreover, the T_c increase from 20 to 25 GPa in Ref. [22] should partially be due to the $N(E_F)$ increase. However, X-ray diffraction measurements show that the cubic phase is pure above 13.44 GPa[16].
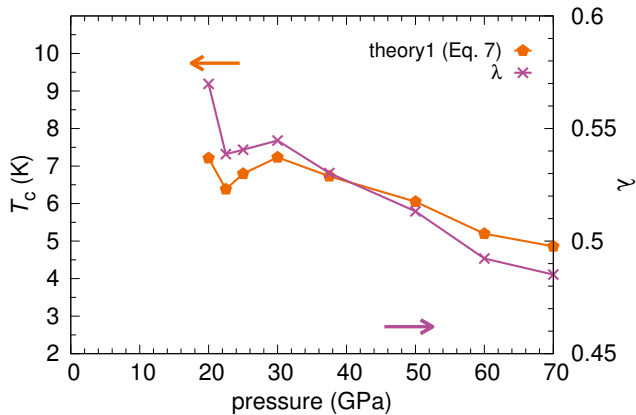
FIG. 18: (Color online) Superconducting transition temperature T_c and $e\text{-}ph$ coupling constant λ as a function of pressure in theoretical calculations using EPW. The adopted μ^* is 0.1.

The adopted structure is rhombohedral in the pressure range from 10 to 20 GPa in calculations[22], which is not consistent with the experimental data from Guo *et al.*[16]. In the simple cubic phase, our conclusion is consistent with that of Ref. 22 that T_c will decrease with increasing pressure (at high pressure).

To estimate if T_c will jump across the phase transition, we perform calculations for phosphorus in simple cubic and rhombohedral (R) phases. As there are unstable phonon modes in the cubic phase at low pressure, we perform the calculations at 22 GPa, near the theoretical phase transition point, where $N(E_F)$ still shows a jump. It can represent the general behavior of T_c during the phase transition. At this pressure, the d band is close to the Fermi level but does not cross it in either phase. The phonon spectra and DOS are shown in Fig. 19 and 20 and their DOS are very similar. In the R phase the phonon modes harden a little and optical modes show a splitting compared with the cubic phase due to additional coupling in the lower-symmetry crystal. If we assume the same effective interaction in the two phases, the $e\text{-}ph$ coupling constant is proportional to $N(E_F)$. Using the McMillan equation, we estimate that the T_c jump is about 1.3 K with with $\mu^* = 0.12$. At the lower pressure, the phonon hardening in the R phase will be larger. The T_c jump will be bigger at the experimental phase transition point because the atomic distortion in the R phase is larger than that in the present calculations. Therefore, when the R phase transforms into the simple cubic phase, T_c will show a jump and it can be mainly attributed to the change of crystal symmetry (affecting the electronic structure and phonon modes) rather than to the Lifshitz transition as suggested in Ref. 22. This is also supported by experimental data which shows that the phase transition (rhombohedral to simple cubic) happens at 12 GPa[16] accompanied by a jump in T_c where the Lifshitz transition cannot occur.

* Electronic address: Xianxin.Wu@physik.uni-wuerzburg.de

[1] J. C. Jamieson, Crystal Structures Adopted by Black Phosphorus at High Pressures, Science **139**, 1291 (1963).

[2] T. Kikegawa and H. Iwasaki, An X-ray Diffraction Study of Lattice Compression and Phase Transition of Crystalline Phosphorus, Acta Cryst. B **39**, 158 (1983).

[3] E. S. Reich, Phosphorene excites materials scientists, Nature **506**, 19 (2014).

[4] H Liu, A. T. Neal, Z. Zhu, Z. Luo, X. F. Xu, D. Tománek, and P. D. Ye, Phosphorene: An Unexplored 2D Semiconductor with a High Hole Mobility, ACS Nano, **8**, 4033 (2014).

[5] L. K. Li, Y. J. Yu, G. J. Ye, Q. Q. Ge, X. D. Ou, H. Wu, D. L. Feng, X. H. Chen and Y. B. Zhang, Black phosphorus field-effect transistors, Nat. Nano. **9**, 372 (2014).

[6] Z. J. Xiang, G. J. Ye, C. Shang, B. Lei, N. Z. Wang, K. S. Yang, D. Y. Liu, F. B. Meng, X. G. Luo, L. J. Zou, Z. Sun, Y. Zhang, and X. H. Chen, Pressure-Induced Electronic Transition in Black Phosphorus, Phys. Rev. Lett. **115**, 186403 (2015).

[7] J. Z. Zhao, R. Yu, H. M. Weng, and Z. Fang, Topological node-line semimetal in compressed black phosphorus, Phys. Rev. B **94**, 195104 (2016).

[8] P. L. Gong, D. Y. Liu, K. S. Yang, Z. J. Xiang, X. H. Chen, Z. Zeng, S. Q. Shen, and L. J. Zou, Hydrostatic pressure induced three-dimensional Dirac semimetal in black phosphorus, Phys. Rev. B **93**, 195434 (2016).

[9] C. H. Li, Y. J. Long, L. X. Zhao, L. Shan, Z. A. Ren, J. Z. Zhao, H. M. Weng, X. Dai, Z. Fang, C. Ren, and G. F. Chen, Pressure-induced topological phase transitions and strongly anisotropic magnetoresistance in bulk black phosphorus, Phys. Rev. B **95**,
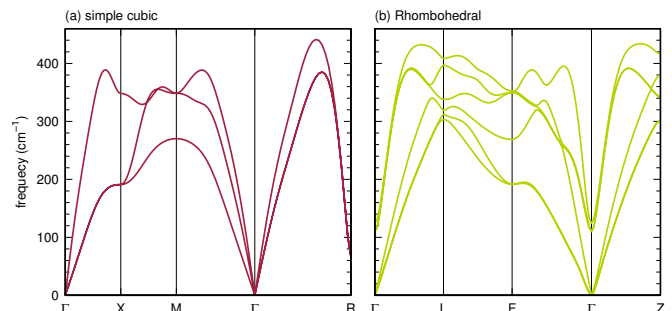
FIG. 19: (Color online) Phonon spectra for the simple cubic and rhombohedral phases at 22 GPa.

125417 (2017).

[10] D.-K. Seo and R. Hoffmann, What Determines the Structures of the Group 15 Elements?, J. Sol. St. Chem. **147**, 26 (1999).

[11] Y. Akahama, M. Kobayashi, and H. Kawamura, Simple-cubic-simple-hexagonal transition in phosphorus under pressure, Phys. Rev. B **59**, 8520 (1999).

[12] J. Wittig, B. Bireckoven, and T. Weidlich, in Solid State Physics Under Pressure, edited by S. Minomura (KTK Scientific, Tokyo,1985), p. 217.

[13] H. Kawamura, I. Shirotani, and K. Tachikawa, Anomalous superconductivity in black phosphorous under high pressures, Solid State Commun. **49**, 879 (1984).

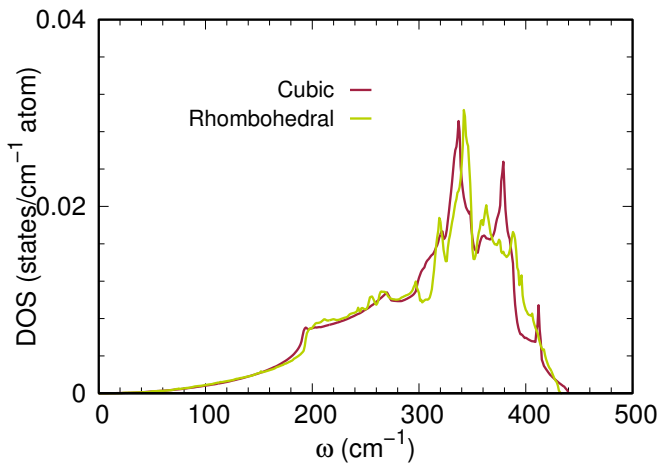[14] H. Kawamura, I. Shirotani, and K. Tachikawa, Anomalous su-

FIG. 20: (Color online) Phonon density of states for the simple cubic and rhombohedral phases at 22 GPa.

perconductivity and pressure induced phase transitions in black phosphorus, Solid State Commun. **54**, 775 (1985).

[15] M. Karuzawa, M. Ishizuka, and S. Endo, The pressure effect on the superconducting transition temperature of black phosphorus, J. Phys.: Condens. Matter **14**, 10759 (2002).

[16] J. Guo, H. H. Wang, F. von Rohr, W. Yi, Y. Zhou, Z. Wang, S. Cai, S. Zhang, X. D. Li, Y. C. Li, J. Liu, K. Yang, A. G. Li, S. Jiang, Q. Wu, T. Xiang, R. J. Cava, L. L. Sun, The vital role of hole-carriers for superconductivity in pressurized black phosphorus, arXiv:1611.03330 (unpublished).

[17] M. Rajagopalan, M. Alouani, and N. E. Christensen, Calculation of Band Structure and Superconductivity in the Simple Cubic Phase of Phosphorus, J. Low Temp. Phys. **75**, 1 (1989).

[18] M. Aoki, N. Suzuki, and K. Motizuki, Electronic Band Structure and Superconductivity in Simple-Cubic Phosphorus, J. Phys. Soc. Jpn. **56**, 3253 (1987).

[19] H. Nagara, K. Mukose, T. Ishikawa, M. Geshi, and N. Suzuki, Origin of the simple modulated structures and the pressure induced superconductivity, J. Phys.: Conf. Series **215**, 012107 (2010).

[20] L. W. Nixon, An investigation of the pressure-induced superconductivity transition temperature T_c and related properties in elemental superconductors, Ph.D. thesis, George Mason University, 2010.

[21] K. T. Chan, B. D. Malone, and M. L. Cohen, Pressure dependence of superconductivity in simple cubic phosphorus, Phys. Rev. B **88**, 064517 (2013).

[22] J. A. Flores-Livas, A. Sanna, A. P. Drozdov, L. Boeri, G. Profeta, M. Eremets, S. Goedecker, Interplay between structure and superconductivity: Metastable phases of phosphorus under pressure Phys. Rev. Materials **1**, 024802 (2017).

[23] P. B. Allen, Neutron Spectroscopy of Superconductors, Phys. Rev. B **6**, 2577 (1972).

[24] A. Y. Liu, I. I. Mazin, and J. Kortus, Beyond Eliashberg Superconductivity in MgB$_2$: Anharmonicity, Two-Phonon Scattering, and Multiple Gaps, Phys. Rev. Lett. **87**, 087005 (2001).

[25] W. L. McMillan, Transition Temperature of Strong-Coupled Su-

perconductors, Phys. Rev. **167**, 331 (1968).

[26] P. B. Allen and R. C. Dynes, Transition temperature of strong-coupled superconductors reanalyzed, Phys. Rev. B **12**, 905 (1975).

[27] P. Morel and P. W. Anderson, Calculation of the Superconducting State Parameters with Retarded Electron-Phonon Interaction, Phys. Rev. **125**, 1263 (1962).

[28] P. B. Allen and B. Mitrovic, Theory of Superconducting T_c, Solid State Physics **37**, 1 (1983).

[29] A. Sanna, S. Pittalis, J. K. Dewhurst, M. Monni, S. Sharma, G. Ummarino, S. Massidda, and E. K. U. Gross, Phononic self-energy effects and superconductivity in CaC$_6$, Phys. Rev. B **85**, 184514 (2012).

[30] P. E. Blöchl, Projector augmented-wave method, Phys. Rev. B **50**, 17953 (1994)

[31] G. Kresse and J. Hafner, *Ab initio* molecular dynamics for liquid metals, Phys. Rev. B **47**, 558 (1993).

[32] G. Kresse and J. Furthmüller, Efficiency of ab-initio total energy calculations for metals and semiconductors using a plane-wave basis set, Comput. Mater. Sci. **6**, 15 (1996).

[33] G. Kresse and J. Furthmüller, Efficient iterative schemes for ab initio total-energy calculations using a plane-wave basis set, Phys. Rev. B **54**, 11169 (1996).

[34] J. P. Perdew, K. Burke, and M. Ernzerhof, Generalized Gradient Approximation Made Simple, Phys. Rev. Lett. **77**, 3865 (1996).

[35] O. K. Andersen, Linear methods in band theory, Phys. Rev. B **12**, 3060 (1975).

[36] The Elk FP-LAPW Code: http://elk.sourceforge.net/.

[37] J. K. Dewhurst, S. Sharma, C. Ambrosch-Draxl, and B. Johansson, First-principles calculation of superconductivity in hole-doped LiBC: T_c = 65 K, Phys. Rev. B **68**, 020504(R) (2003).

[38] K. Koepernik and H. Eschrig, Full-potential nonorthogonal local-orbital minimum-basis band-structure scheme, Phys. Rev. B **59**, 1743 (1999).

[39] F. Giustino, M. L. Cohen, and S. G. Louie, Electron-phonon interaction using Wannier functions, Phys. Rev. B **76**, 165108 (2007).

[40] S. Poncé, E. R. Margine, C. Verdia and F. Giustino, EPW: Electronphonon coupling, transport and superconducting properties using maximally localized Wannier functions, Comput. Phys. Commun. **209**, 116 (2016).

[41] P. Giannozzi *et al.*, QUANTUM ESPRESSO: a modular and open-source software project for quantum simulations of materials, J. Phys.:Condens. Matter **21**, 395502 (2009).

[42] S. M. Clark and J. M. Zaug, Compressibility of cubic white, orthorhombic black, rhombohedral black, and simple cubic black phosphorus, Phys. Rev. B **82**, 134111 (2010).

[43] M. Monni, F. Bernardini, A. Sanna, G. Profeta, and S. Massidda, Origin of the critical temperature discontinuity in superconducting sulfur under high pressure, Phys. Rev. B **95**, 064516 (2017).

[44] J. Ziman, Electrons and Phonons, Oxford University Press (1960).

[45] R. Akashi and R. Arita, Development of Density-Functional Theory for a Plasmon-Assisted Superconducting State: Application to Lithium Under High Pressures, Phys. Rev. Lett. **111** 057006 (2013).

[46] A. V. Krukau , O. A. Vydrov, A. F. Izmaylov, and G. E. Scuseria, Influence of the exchange screening parameter on the performance of screened hybrid functionals, J. Chem. Phys. **125**, 224106 (2006).